Determination of geosynthetic constitutive parameters and soil/geosynthetic interaction by in-air and in-soil experiments
by Eli Vincent Cuelho

A thesis submitted in partial fulfillment of the requirements for the degree of Master of Science in Civil Engineering
Montana State University

Abstract:
In recent years geogrids and geotextiles have been evaluated for use as reinforcement in the base course layer of flexible pavement structures. Adding reinforcement to the base layer can help reduce the thickness of the base material or increase the life of the roadway. To understand and quantify potential reinforcement benefit, a program of study that relies on both experimental and modeling studies was devised. The increased use of finite element modeling to simulate material and system behavior has also increased the need for more specialized tests performed on the model components.

The focus of this research was to develop test methods and provide data that can be used for the calibration of constitutive models that describe geosynthetic material parameters and soil/geosynthetic interaction parameters. Calibration of geosynthetic material models required that elastic, inelastic, viscous, direction dependant and repetitive load dependant material properties be defined. To define the soil/geosynthetic interaction characteristics, insoil (confined) tests were performed.

A large scale test facility was designed and built for performing both in-air and in-soil experiments on geosynthetics. In-air, displacement-rate controlled (monotonic) and load controlled (cyclic) tests on the geosynthetic material allowed orthotropic elastic and isotropic yield material properties to be obtained. Monotonic pull-out tests were performed at three levels of normal confinement to calibrate soil/geosynthetic interaction parameters. Several common methods of interpreting the data from these tests were examined, but, due to complications associated with these methods, a numerical solution of the governing differential equation, which describes the interaction problem, was formulated.

Determination of Geosynthetic Constitutive Parameters and Soil/Geosynthetic Interaction by In-Air and In-Soil Experiments

by

Eli Vincent Cuelho

A thesis submitted in partial fulfillment
of the requirements for the degree

of

Master of Science

in

Civil Engineering

MONTANA STATE UNIVERSITY
Bozeman, Montana

May, 1998

APPROVAL

of a thesis submitted by

Eli Vincent Cuelho

This thesis has been read by each member of the thesis committee and has been found to be satisfactory regarding content, English usage, format, citations, bibliographic style, and consistency, and is ready for submission to the College of Graduate Studies.

Dr. Steven Perkins — (Signature) — 5-12-98 Date

Approved for the Department of Civil Engineering

Dr. Don Rabern — Donald A. Rabern (Signature) — 5/12/98 Date

Approved for the College of Graduate Studies

Dr. Joseph Fedock — Joseph J. Fedock (Signature) — 5/14/98 Date

STATEMENT OF PERMISSION TO USE

In presenting this thesis in partial fulfillment of the requirements for a Master's degree at Montana State University - Bozeman, I agree that the library shall make it available to borrowers under rules of the Library.

If I have indicated my intention to copyright this thesis by including a copyright notice page, copying is allowable only for scholarly purposes, consistent with "fair use" as prescribed in the U.S. Copyright Law. Requests for permission for extended quotation from or reproduction of this thesis in whole or in parts may be granted only by the copyright holder.

Signature 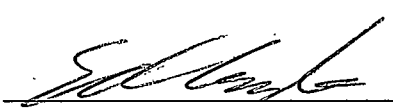

Date May 12, 1998

ACKNOWLEDGMENTS

First I would like to express my utmost appreciation to my wife Bobbie, and my five children, Beker, Blu, Ira, Ezra and Hanoch, who have patiently supported and encouraged me every step along the way. I would also like to personally thank my close friends who were a constant encouragement to me through their continual prayers to G-d. I would like to recognize the outstanding contribution made by Dr. Steve Perkins through his accessibility, assistance and support, and my committee members, Dr. Don Rabern and Dr. Jim Dent, for their timely advice during this study.

I would like to thank Gordon Williamson for his meticulous work in helping me to construct the pull-out test facility, Wes Harms for allowing me to use his tools to maintain and operate the test apparatus, Yan Wang for helping me with the computer programs to reduce experimental data and Phil Gyr for tirelessly proofreading this document. Also, a big thank you to Bridge Diagnostics, Inc. and Chris Clark for setting up and maintaining the data acquisition system.

The financial support for this study was provided through a grant supplied by the Montana Department of Transportation. Amoco and Tensar Corporations graciously donated the geosynthetic materials used in this study.

Last, but certainly not least, I would like to thank my Rock and my Redeemer, the G-d of Israel, for giving me the strength to complete this work and for being my ever present help in time of need.

שמע ישראל יי אלהינו יי אחד

TABLE OF CONTENTS

Page

1. INTRODUCTION 1

Background 1
Scope of Work 2
Experimentation 3
In-Air Tests 4
In-Soil Tests 5
Organization of Thesis 6

2. LITERATURE REVIEW 7

Introduction 7
In-Air Testing 7
In-Soil Testing 12
Direct Shear Devices 13
Pull-Out Test Devices 15
Pull-Out Apparatus Design 16
Loading Methods 16
Boundary Conditions 18
Gap Interface 19
Walls 21
Top 24
Analysis of Pull-Out Results 26
Mobilizing Process Method 26
Average Resistance Method 31
Total Area Method 33
Effective Area Method 33
Maximum Slope Method 34
Numerical Method 35
Finite Element Modeling 38

TABLE OF CONTENTS -- Continued

Page

3. EXPERIMENTAL METHODS AND TEST RESULTS 40

Introduction 40
Design Considerations 40
Equipment Description 42
Displacement-Rate Controlled Pulling Mechanism 43
Load Controlled Pulling Mechanism 43
Clamping Method 44
Instrumentation and System Controls 44
In-Soil, Pull-Out, Apparatus 46
Gap Interface 46
Walls 48
Top 49
In-Air Apparatus 49
Test Procedures 51
In-Air Test Procedures 51
Sample Preparation 52
Loading Device and Instrumentation Connection 58
Fast Monotonic Tests 59
Slow Monotonic Tests 59
Cyclic Tests 59
In-Soil Test Procedures 61
Sample Preparation 62
Soil Compaction and Sample Placement 63
Loading Device and Instrumentation Connection 66
Normal Confinement 67
Conducting the Test 67
Monotonic Tests 68
Cyclic Tests 68
Test Results 69
In-Air Test Results 69

TABLE OF CONTENTS -- Continued

Page

Test Data Corrections 69
Fast, Monotonic, In-Air Tests 71
Slow, Monotonic, In-Air Tests 71
Cyclic, In-Air Tests 74
In-Soil Test Results 74
Test Data Corrections 76
Monotonic, In-Soil Tests 77
Cyclic, In-Soil Tests 79

4. DISCUSSION AND ANALYSIS OF TEST RESULTS 82

Introduction 82
Discussion of In-Air Test Results 83
Analysis of In-Air Test Results 87
Discussion of In-Soil (Pull-Out) Test Results 91
Analysis of In-Soil (Pull-Out) Test Results 93
Mobilizing Process Method 94
Approximating the Displacement Distribution 94
Determining Strains in the Material 97
Determining Load in the Material 97
Results 100
Numerical Method 103
Derivation of Differential Equation 104
Definition of Functions and Variables in Differential Equation 104
Solution of Equation 108
Boundary Conditions 109
Numerical Analysis 110
General Solution 111
Calibration of Solution 112
Results fron Numerical Analysis 113

TABLE OF CONTENTS -- Continued

Page

5. SUMMARY, CONCLUSIONS AND RECOMMENDATIONS FOR FURTHER RESEARCH 124

Summary 124
Conclusion 125
Recommendations for Further Research 127
Design and Operation of Test Facility 128
Sample Preparation and Testing 129
Data Interpretation 131

BIBLIOGRAPHY 132

APPENDICES 144

Appendix A: Installation of Geosynthetic Bonded Resistance Strain Gages . 145
Introduction 146
Gage Description 146
Gage Placement 147
Geogrid Gage Placement Procedure 148
Geotextile Gage Placement Procedure 151
Results 153
Appendix B: Complete Results from the In-Air and In-Soil Tests 160
Appendix C: Complete Results from the In-Soil Analysis 201
Appendix D: List of Equipment Sources 226

LIST OF TABLES

Page

Table 3.1: Material properties of the geogrid and geotextile as reported by the manufacturer 52

Table 3.2: Cycle numbers repeated at each load level for the in-air, cyclic, Series II tests 61

Table 3.3: Cycle numbers repeated at each load level for the in-soil, cyclic tests 68

Table 4.1: In-air constitutive material parameters for the geogrid 90

Table 4.2: In-air constitutive material parameters for the geotextile 90

Table 4.3: Interaction parameters for the geogrid and geotextile 118

Table B.1: Cycle numbers collected and plotted for the in-air, cyclic, Series II tests 168

Table B.2: Cycle numbers collected and plotted for the in-soil, cyclic, Series II tests 186

LIST OF FIGURES

Page

Figure 2.1: Change in tensile modulus for different specimen widths in Geolon 1250 geotextile (Rowe and Ho, 1986) 9

Figure 2.2: Variations of maximum tensile strength under different strain rates (Rowe and Ho, 1986) 9

Figure 2.3: Changes in load/strain properties for different loading rates in HDPE and PET geogrids (Bathurst and Cai, 1994) 10

Figure 2.4: Change in load/strain properties in a HDPE geogrid due to changes in frequency for cyclic loading (Bathurst and Cai, 1994) 11

Figure 2.5: Clamping systems (Myles, 1987) 11

Figure 2.6: Temperature effect on the cyclic load/strain properties of a HDPE geogrid (Moraci and Montanelli, 1996) 12

Figure 2.7: Shear box types (Richards and Scott, 1985) 14

Figure 2.8: Three principle mechanisms of soil/geosynthetic interaction (Jewell et al., 1984) 16

Figure 2.9: Effects of rate of pull on pull-out resistance (Yasuda et al., 1992) 17

Figure 2.10: Effect of load-transfer sleeve length on pull-out resistance of geogrid (Farrag, 1991) 21

Figure 2.11: Effect of front wall friction on normalized pull-out resistance for a geogrid (Palmeira and Milligan, 1989) 22

Figure 2.12: Effect of side-wall friction on vertical pressure (Farrag, 1991) 23

Figure 2.13: Effect of specimen width on pull-out resistance (after Ochiai et al., 1996) 23

LIST OF FIGURES -- Continued

Page

Figure 2.14: Effects of top boundary on pull-out resistance (Palmeira and Milligan, 1989) 25

Figure 2.15: Effect of depth of soil, above and below reinforcement, on pull-out resistance (Farrag, 1991) 25

Figure 2.16: Graphical representation of the mobilizing process method (Ochiai et al., 1996) 27

Figure 2.17: Concepts in evaluating pull-out resistance using the mobilizing process method (redrawn after Ochiai et al., 1996) 28

Figure 2.18: Free-body diagram of shear calculation 31

Figure 2.19: Three average resistance methods used to evaluate pull-out resistance (Ochiai et al., 1996) 32

Figure 2.20: Graphical representation of the methods used to evaluate pull-out resistance (Ochiai et al., 1996) 32

Figure 2.21: Effect of analysis method on average pull-out resistance (Ochiai et al., 1996) 35

Figure 3.1: Plan view of test apparatus 43

Figure 3.2: Front view of pull-out apparatus showing gap formed by separated upper and lower halves 47

Figure 3.3: Orientation, dimensions and method of attachment of load-transfer sleeves at the front wall 47

Figure 3.4: Schematic of normal confinement apparatus: a) view from end b) view from side 50

Figure 3.5: Schematic of in-air specimen showing overall dimensions and sensor location 54

LIST OF FIGURES -- Continued

Page

Figure 3.6: Sample jig for preparing in-air test specimens 55

Figure 3.7: Side view of in-air sample clamping method including loadcell connection 56

Figure 3.8: Plan view of sample clamping method including loadcell connection 57

Figure 3.9: Load history of a single input load cycle 60

Figure 3.10: Load levels for the cyclic load input pulses 60

Figure 3.11: In-soil sample placed in pull-out box 62

Figure 3.12: Grain-size distribution of the confinement soil used in pull-out experiments 64

Figure 3.13: Modified Proctor compaction curve for soil used in pull-out experiments 64

Figure 3.14: Plan view of in-soil sample arrangement 65

Figure 3.15: Fast, monotonic, load/strain curves for the geogrid and the geotextile in both principle strength directions 72

Figure 3.16: Fast, monotonic axial strain versus lateral strain for the geogrid and geotextile in both principle strength directions 72

Figure 3.17: Slow, monotonic, load/strain curves for the geogrid and the geotextile in both principle strength directions 73

Figure 3.18: Slow, monotonic axial strain versus lateral strain for the geogrid and geotextile in both principle strength directions 73

Figure 3.19: Cyclic, Series I, load/strain, loading/unloading curves for the geogrid in the machine direction: ggmd-3 75

LIST OF FIGURES -- Continued

Page

Figure 3.20: Cyclic, Series II, load/strain, loading/unloading curves for the geogrid in the machine direction: ggmd-6 75

Figure 3.21: Averaged load versus displacement curves for the in-soil, sheet metal tests 77

Figure 3.22: In-soil, load versus displacement curves for the geogrid pulled in the machine direction at three levels of normal confinement 78

Figure 3.23: In-soil displacement versus distance along reinforcement length for geogrid pulled in the machine direction at 5 kPa normal confinement: ggmd-12 78

Figure 3.24: Maximum and minimum loads applied to the geogrid in the machine direction at 15 kPa normal confinement: ggmd-13 80

Figure 3.25: Maximum and minimum displacement at the front of a sample of geogrid pulled in the machine direction at 15 kPa normal confinement: ggmd-13 80

Figure 3.26: Cyclic, in-soil, unloading/reloading load/displacement curves for a sample of geogrid pulled in the machine direction at 15 kPa normal confinement: ggmd-13 81

Figure 4.1: Comparison between fast and slow monotonic tests performed on the geogrid in the machine direction 85

Figure 4.2: Comparison between fast and slow monotonic tests performed on the geotextile in the machine direction 85

Figure 4.3: Comparison between fast monotonic and cyclic, Series I tests performed on the geogrid in the machine direction 86

Figure 4.4: Comparison between slow monotonic and cyclic, Series II tests performed on the geogrid in the machine direction 86

LIST OF FIGURES -- Continued

Page

Figure 4.5: Comparison of monotonic and cyclic pull-out tests performed on the geogrid in the machine direction at 15 kPa normal confinement . . 92

Figure 4.6: Approximations of a displacement distribution using linear, cubic spline and sum-of-exponentials approaches 96

Figure 4.7: Strain distributions calculated using a linear, cubic spline and sum-of-exponentials approximation of a displacement distribution 96

Figure 4.8: Comparison of in-air and in-soil load/strain curves for the geogrid pulled in the machine direction 98

Figure 4.9: Free-body diagram of shear interaction 100

Figure 4.10: Shear stress versus shear displacement for the geogrid pulled in the machine direction at a normal confinement of 5 kPa; computed using a linear approximation of the displacement distribution 102

Figure 4.11: Shear stress versus shear displacement for the geogrid pulled in the machine direction at a normal confinement of 5 kPa; computed using a sum-of-exponentials approximation of the displacement distribution 102

Figure 4.12: Curve fit approximations of the in-air, load/strain curves for the geogrid 107

Figure 4.13: Curve fit approximations of the in-air, load/strain curves for the geotextile 107

Figure 4.14: Generic shear stress versus shear displacement curve 109

Figure 4.15: Comparison of Level I displacements for the geotextile pulled in the machine direction at 35 kPa normal confinement: gtxd-15 . . . 114

Figure 4.16: Comparison of Level II displacements for the geotextile pulled in the machine direction at 35 kPa normal confinement: gtxd-15 . . . 114

LIST OF FIGURES -- Continued

Page

Figure 4.17: Comparison of Level III displacements for the geotextile pulled in the machine direction at 35 kPa normal confinement: gtxd-15 ... 115

Figure 4.18: Comparison of Level IV displacements for the geotextile pulled in the machine direction at 35 kPa normal confinement: gtxd-15 ... 115

Figure 4.19: Comparison of Level V displacements for the geotextile pulled in the machine direction at 35 kPa normal confinement: gtxd-15 ... 116

Figure 4.20: Comparison of Level VI displacements for the geotextile pulled in the machine direction at 35 kPa normal confinement: gtxd-15 ... 116

Figure 4.21: Comparison between actual and predicted load/displacement curves for the geotextile pulled in the machine direction at 35 kPa normal confinement: gtxd-15 ... 117

Figure 4.22: Predicted shear stress versus shear displacement curve for the geotextile pulled in the machine direction at 35 kPa normal confinement: gtxd-15 ... 117

Figure 4.23: Ultimate and residual shear stress versus normal confinement curves for the geogrid ... 120

Figure 4.24: Ultimate and residual shear stress versus normal confinement curves for the geotextile ... 120

Figure 4.25: Initial interface shear moduli versus normal confinement for the geogrid and the geotextile ... 122

Figure A.1: The two types of foil strain gages used a) geogrid strain gage and b) geotextile strain gage ... 147

Figure A.2: Wheatstone bridge circuit ... 150

Figure A.3: Comparison of the foil and axial strain results from slow monotonic tests performed on the geogrid in the machine direction ... 155

LIST OF FIGURES -- Continued

Page

Figure A.4: Comparison of the foil and axial strain results from slow monotonic tests performed on the geogrid in the cross-machine direction 155

Figure A.5: Comparison of the foil and axial strain results from slow monotonic tests performed on the geotextile in the cross-machine direction 156

Figure A.6: Comparison of the foil and axial strain results from a cyclic, Series I test performed on the geogrid in the machine direction (ggmd-3) 156

Figure A.7: Comparison of the foil and axial strain results from a cyclic, Series I test performed on the geogrid in the cross-machine direction (ggxd-4) 157

Figure A.8: Comparison of the foil and axial strain results from a cyclic, Series I test performed on the geotextile in the machine direction (gtmd-4) .. 157

Figure A.9: Comparison of the foil and axial strain results from a cyclic, Series I test performed on the geotextile in the cross-machine direction (gtxd-3) 158

Figure A.10: Comparison of the foil and axial strain results from a cyclic, Series II test performed on the geogrid in the machine direction (ggmd-6) ... 158

Figure A.11: Comparison of the foil and axial strain results from a cyclic, Series II test performed on the geotextile in the machine direction (gtmd-5) 159

Figure A.12: Comparison of the foil and axial strain results from a cyclic, Series II test performed on the geotextile in the cross-machine direction (gtxd-5) 159

Figure B.1: Fast, monotonic, load/strain curves for the geogrid pulled in the machine and cross-machine directions 161

LIST OF FIGURES -- Continued

Page

Figure B.2: Slow, monotonic, load/strain curves for the geogrid pulled in the machine and cross-machine directions 161

Figure B.3: Fast, monotonic, load/strain curves for the geotextile pulled in the machine and cross-machine directions 162

Figure B.4: Slow, monotonic, load/strain curves for the geotextile pulled in the machine and cross-machine directions 162

Figure B.5: Fast, monotonic axial strain versus lateral strain curves for the geogrid pulled in the machine and cross-machine directions 163

Figure B.6: Slow, monotonic axial strain versus lateral strain curves for the geogrid pulled in the machine and cross-machine directions 163

Figure B.7: Fast, monotonic axial strain versus lateral strain curves for the geotextile pulled in the machine and cross-machine directions 164

Figure B.8: Slow, monotonic axial strain versus lateral strain curves for the geotextile pulled in the machine and cross-machine directions 164

Figure B.9: Load versus axial strain in the geogrid oriented at 45 degrees from its principle strength directions: gg45-1 165

Figure B.10: Axial strain versus lateral strain in the geogrid oriented at 45 degrees from its principle strength directions: gg45-1 165

Figure B.11: Cyclic, Series I, unloading/reloading, load/strain curves for the geogrid pulled in the machine direction: ggmd-3 166

Figure B.12: Cyclic, Series I, unloading/reloading, load/strain curves for the geogrid pulled in the cross-machine direction: ggxd-4 166

Figure B.13: Cyclic, Series I, unloading/reloading, load/strain curves for the geotextile pulled in the machine direction: gtmd-4 167

LIST OF FIGURES -- Continued

Page

Figure B.14: Cyclic, Series I, unloading/reloading, load/strain curves for the geotextile pulled in the cross-machine direction: gtxd-3 167

Figure B.15: Cyclic, Series II, unloading/reloading, load/strain curves for the geogrid pulled in the machine direction: ggmd-5 169

Figure B.16: Cyclic, Series II, unloading/reloading, load/strain curves for the geogrid pulled in the machine direction: ggmd-6 169

Figure B.17: Cyclic, Series II, unloading/reloading, load/strain curves for the geogrid pulled in the cross-machine direction: ggxd-3 170

Figure B.18: Cyclic, Series II, unloading/reloading, load/strain curves for the geotextile pulled in the machine direction: gtmd-5 170

Figure B.19: Cyclic, Series II, unloading/reloading, load/strain curves for the geotextile pulled in the cross-machine direction: gtxd-4 171

Figure B.20: Cyclic, Series II, unloading/reloading, load/strain curves for the geotextile pulled in the cross-machine direction: gtxd-5 171

Figure B.21: Maximum and minimum loads applied to the geogrid in the machine direction for an in-air, cyclic, Series II test: ggmd-5 172

Figure B.22: Maximum and minimum loads applied to the geogrid in the machine direction for an in-air, cyclic, Series II test: ggmd-6 172

Figure B.23: Maximum and minimum loads applied to the geogrid in the cross-machine direction for an in-air, cyclic, Series II test: ggxd-3 173

Figure B.24: Maximum and minimum loads applied to the geotextile in the machine direction for an in-air, cyclic, Series II test: ggmd-5 173

Figure B.25: Maximum and minimum loads applied to the geotextile in the cross-machine direction for an in-air, cyclic, Series II test: gtxd-4 174

LIST OF FIGURES -- Continued

Page

Figure B.26: Maximum and minimum loads applied to the geotextile in the cross-machine direction for an in-air, cyclic, Series II test: gtxd-5 174

Figure B.27: Maximum and minimum axial strains of the geogrid pulled in the machine direction for an in-air, cyclic, Series II test: ggmd-5 . . . 175

Figure B.28: Maximum and minimum axial strains of the geogrid pulled in the machine direction for an in-air, cyclic, Series II test: ggmd-6 . . . 175

Figure B.29: Maximum and minimum axial strains of the geogrid pulled in the cross-machine direction for an in-air, cyclic, Series II test: ggxd-3 176

Figure B.30: Maximum and minimum axial strains of the geotextile pulled in the machine direction for an in-air, cyclic, Series II test: gtmd-5 176

Figure B.31: Maximum and minimum axial strains of the geotextile pulled in the cross- machine direction for an in-air, cyclic, Series II test: gtxd-4 177

Figure B.32: Maximum and minimum axial strains of the geotextile pulled in the cross- machine direction for an in-air, cyclic, Series II test: gtxd-5 177

Figure B.33: In-soil, load/displacement curves for the geogrid pulled in the machine direction for three levels of normal confinement 178

Figure B.34: Displacement along the length of the geogrid pulled in the machine direction at 5 kPa normal confinement: ggmd-12 178

Figure B.35: Displacement along the length of the geogrid pulled in the machine direction at 15 kPa normal confinement: ggmd-11 179

Figure B.36: Displacement along the length of the geogrid pulled in the machine direction at 35 kPa normal confinement: ggmd-10 179

Figure B.37: In-soil, load/displacement curves for the geogrid pulled in the cross-machine direction for three levels of normal confinement 180

LIST OF FIGURES -- Continued

Page

Figure B.38: Displacement along the length of the geogrid pulled in the cross-machine direction at 5 kPa normal confinement: ggxd-9 180

Figure B.39: Displacement along the length of the geogrid pulled in the cross-machine direction at 15 kPa normal confinement: ggxd-8 181

Figure B.40: Displacement along the length of the geogrid pulled in the cross-machine direction at 35 kPa normal confinement: ggxd-7 181

Figure B.41: In-soil, load/displacement curves for the geotextile pulled in the machine direction for three levels of normal confinement 182

Figure B.42: Displacement along the length of the geotextile pulled in the machine direction at 5 kPa normal confinement: gtmd-14 182

Figure B.43: Displacement along the length of the geotextile pulled in the machine direction at 15 kPa normal confinement: gtmd-12 183

Figure B.44: Displacement along the length of the geotextile pulled in the machine direction at 35 kPa normal confinement: gtmd-13 183

Figure B.45: In-soil, load/displacement curves for the geotextile pulled in the cross- machine direction for three levels of normal confinement 184

Figure B.46: Displacement along the length of the geotextile pulled in the cross-machine direction at 5 kPa normal confinement: gtxd-13 184

Figure B.47: Displacement along the length of the geotextile pulled in the cross-machine direction at 15 kPa normal confinement: gtxd14 185

Figure B.48: Displacement along the length of the geotextile pulled in the cross-machine direction at 35 kPa normal confinement: gtxd-15 185

Figure B.49: Cyclic, in-soil, unloading/reloading load/displacement curves for the geogrid pulled in the machine direction at 15 kPa normal confinement: ggmd-13 187

LIST OF FIGURES -- Continued

Page

Figure B.50: Cyclic, in-soil, unloading/reloading load/displacement curves for the geogrid pulled in the cross-machine direction at 15 kPa normal confinement: ggxd-10 187

Figure B.51: Cyclic, in-soil, unloading/reloading load/displacement curves for the geotextile pulled in the machine direction at 15 kPa normal confinement: gtmd-15 188

Figure B.52: Cyclic, in-soil, unloading/reloading load/displacement curves for the geotextile pulled in the cross-machine direction at 15 kPa normal confinement: gtxd-16 188

Figure B.53: Maximum and minimum loads applied to the geogrid in the machine direction at 15 kPa normal confinement for an in-soil, cyclic, Series II test: ggmd-13 189

Figure B.54: Maximum and minimum displacements at the front of a sample of geogrid pulled in the machine direction at 15 kPa normal confinement for an in-soil, cyclic, Series II test: ggmd-13 189

Figure B.55: Maximum and minimum displacements at position two along the length of a sample of geogrid pulled in the machine direction at 15 kPa normal confinement for an in-soil, cyclic, Series II test: ggmd-13 ... 190

Figure B.56: Maximum and minimum displacements at position three along the length of a sample of geogrid pulled in the machine direction at 15 kPa normal confinement for an in-soil, cyclic, Series II test: ggmd-13 ... 190

Figure B.57: Maximum and minimum displacements at position four along the length of a sample of geogrid pulled in the machine direction at 15 kPa normal confinement for an in-soil, cyclic, Series II test: ggmd-13 ... 191

Figure B.58: Maximum and minimum displacements at position five along the length of a sample of geogrid pulled in the machine direction at 15 kPa normal confinement for an in-soil, cyclic, Series II test: ggmd-13 ... 191

LIST OF FIGURES -- Continued

Page

Figure B.59: Maximum and minimum loads applied to the geogrid in the cross-machine direction at 15 kPa normal confinement for an in-soil, cyclic, Series II test: ggxd-10 192

Figure B.60: Maximum and minimum displacements at the front of a sample of geogrid pulled in the cross-machine direction at 15 kPa normal confinement for an in-soil, cyclic, Series II test: ggxd-10 192

Figure B.61: Maximum and minimum displacements at position two along the length of a sample of geogrid pulled in the cross-machine direction at 15 kPa normal confinement for an in-soil, cyclic, Series II test: ggxd-10 193

Figure B.62: Maximum and minimum displacements at position three along the length of a sample of geogrid pulled in the cross-machine direction at 15 kPa normal confinement for an in-soil, cyclic, Series II test: ggxd-10 193

Figure B.63: Maximum and minimum displacements at position four along the length of a sample of geogrid pulled in the cross-machine direction at 15 kPa normal confinement for an in-soil, cyclic, Series II test: ggxd-10 194

Figure B.64: Maximum and minimum displacements at position five along the length of a sample of geogrid pulled in the cross-machine direction at 15 kPa normal confinement for an in-soil, cyclic, Series II test: ggxd-10 194

Figure B.65: Maximum and minimum loads applied to the geotextile in the machine direction at 15 kPa normal confinement for an in-soil, cyclic, Series II test: gtmd-15 195

Figure B.66: Maximum and minimum displacements at the front of a sample of geotextile pulled in the machine direction at 15 kPa normal confinement for an in-soil, cyclic, Series II test: gtmd-15 195

LIST OF FIGURES -- Continued

Page

Figure B.67: Maximum and minimum displacements at position two along the length of a sample of geotextile pulled in the machine direction at 15 kPa normal confinement for an in-soil, cyclic, Series II test: gtmd-15 196

Figure B.68: Maximum and minimum displacements at position three along the length of a sample of geotextile pulled in the machine direction at 15 kPa normal confinement for an in-soil, cyclic, Series II test: gtmd-15 196

Figure B.69: Maximum and minimum displacements at position four along the length of a sample of geotextile pulled in the machine direction at 15 kPa normal confinement for an in-soil, cyclic, Series II test: gtmd-15 197

Figure B.70: Maximum and minimum displacements at position five along the length of a sample of geotextile pulled in the machine direction at 15 kPa normal confinement for an in-soil, cyclic, Series II test: gtmd-15 197

Figure B.71: Maximum and minimum loads applied to the geotextile in the cross-machine direction at 15 kPa normal confinement for an in-soil, cyclic, Series II test: gtxd-16 198

Figure B.72: Maximum and minimum displacements at the front of a sample of geotextile pulled in the cross-machine direction at 15 kPa normal confinement for an in-soil, cyclic, Series II test: gtxd-16 198

Figure B.73: Maximum and minimum displacements at position two along the length of a sample of geotextile pulled in the cross-machine direction at 15 kPa normal confinement for an in-soil, cyclic, Series II test: gtxd-16 199

Figure B.74: Maximum and minimum displacements at position three along the length of a sample of geotextile pulled in the cross-machine direction at 15 kPa normal confinement for an in-soil, cyclic, Series II test: gtxd-16 199

LIST OF FIGURES -- Continued

Page

Figure B.75: Maximum and minimum displacements at position four along the length of a sample of geotextile pulled in the cross-machine direction at 15 kPa normal confinement for an in-soil, cyclic, Series II test: gtxd-16 200

Figure B.76: Maximum and minimum displacements at position five along the length of a sample of geotextile pulled in the cross-machine direction at 15 kPa normal confinement for an in-soil, cyclic, Series II test: gtxd-16 200

Figure C.1: Comparisons between actual and predicted displacement curves for the geogrid pulled in the machine direction at σ_n=5 kPa: a) Level I, b) Level II, c) Level III, d) Level IV, e) Level V, f) Level VI: ggmd-12 202

Figure C.2: Comparison between actual and predicted load/displacement curves for the geogrid pulled in the machine direction at σ_n=5 kPa: ggmd-12 203

Figure C.3: Predicted shear stress versus shear displacement curve for the geogrid pulled in the machine direction at σ_n=5 kPa: ggmd-12 203

Figure C.4: Comparisons between actual and predicted displacement curves for the geogrid pulled in the machine direction at σ_n=15 kPa: a) Level I, b) Level II, c) Level III, d) Level IV, e) Level V, f) Level VI: ggmd-11 204

Figure C.5: Comparison between actual and predicted load/displacement curves for the geogrid pulled in the machine direction at σ_n=15 kPa: ggmd-11 205

Figure C.6: Predicted shear stress versus shear displacement curve for the geogrid pulled in the machine direction at σ_n=15 kPa: ggmd-11 205

LIST OF FIGURES -- Continued

Page

Figure C.7: Comparisons between actual and predicted displacement curves for the geogrid pulled in the machine direction at σ_n=35 kPa: a) Level I, b) Level II, c) Level III, d) Level IV, e) Level V, f) Level VI: ggmd-10 206

Figure C.8: Comparison between actual and predicted load/displacement curves for the geogrid pulled in the machine direction at σ_n=35 kPa: ggmd-10 207

Figure C.9: Predicted shear stress versus shear displacement curve for the geogrid pulled in the machine direction at σ_n=35 kPa: ggmd-10 207

Figure C.10: Comparisons between actual and predicted displacement curves for the geogrid pulled in the cross-machine direction at σ_n=5 kPa: a) Level I, b) Level II, c) Level III, d) Level IV, e) Level V, f) Level VI: ggxd-9 208

Figure C.11: Comparison between actual and predicted load/displacement curves for the geogrid pulled in the cross-machine direction at σ_n=5 kPa: ggxd-9 209

Figure C.12: Predicted shear stress versus shear displacement curve for the geogrid pulled in the cross-machine direction at σ_n=5 kPa: ggxd-9 .. 209

Figure C.13: Comparisons between actual and predicted displacement curves for the geogrid pulled in the cross-machine direction at σ_n=15 kPa: a) Level I, b) Level II, c) Level III, d) Level IV, e) Level V, f) Level VI: ggxd-8 210

Figure C.14: Comparison between actual and predicted load/displacement curves for the geogrid pulled in the cross-machine direction at σ_n=15 kPa: ggxd-8 211

Figure C.15: Predicted shear stress versus shear displacement curve for the geogrid pulled in the cross-machine direction at σ_n=15 kPa: ggxd-8 211

LIST OF FIGURES -- Continued

Page

Figure C.16: Comparisons between actual and predicted displacement curves for the geogrid pulled in the cross-machine direction at σ_n=35 kPa: a) Level I, b) Level II, c) Level III, d) Level IV, e) Level V, f) Level VI: ggxd-7 212

Figure C.17: Comparison between actual and predicted load/displacement curves for the geogrid pulled in the cross-machine direction at σ_n=35 kPa: ggxd-7 213

Figure C.18: Predicted shear stress versus shear displacement curve for the geogrid pulled in the cross-machine direction at σ_n=35 kPa: ggxd-7 213

Figure C.19: Comparisons between actual and predicted displacement curves for the geotextile pulled in the machine direction at σ_n=5 kPa: a) Level I, b) Level II, c) Level III, d) Level IV, e) Level V, f) Level VI: gtmd-14 214

Figure C.20: Comparison between actual and predicted load/displacement curves for the geotextile pulled in the machine direction at σ_n=5 kPa: gtmd-14 215

Figure C.21: Predicted shear stress versus shear displacement curve for the geotextile pulled in the machine direction at σ_n=5 kPa: gtmd-14 ... 215

Figure C.22: Comparisons between actual and predicted displacement curves for the geotextile pulled in the machine direction at σ_n=15 kPa: a) Level I, b) Level II, c) Level III, d) Level IV, e) Level V, f) Level VI: gtmd-12 216

Figure C.23: Comparison between actual and predicted load/displacement curves for the geotextile pulled in the machine direction at σ_n=15 kPa: gtmd-12 217

LIST OF FIGURES -- Continued

Page

Figure C.24: Predicted shear stress versus shear displacement curve for the geotextile pulled in the machine direction at σ_n=15 kPa: gtmd-12 . . 217

Figure C.25: Comparisons between actual and predicted displacement curves for the geotextile pulled in the machine direction at σ_n=35 kPa: a) Level I, b) Level II, c) Level III, d) Level IV, e) Level V, f) Level VI: gtmd-13 218

Figure C.26: Comparison between actual and predicted load/displacement curves for the geotextile pulled in the machine direction at σ_n=35 kPa: gtmd-13 219

Figure C.27: Predicted shear stress versus shear displacement curve for the geotextile pulled in the machine direction at σ_n=35 kPa: gtmd-13 219

Figure C.28: Comparisons between actual and predicted displacement curves for the geotextile pulled in the cross-machine direction at σ_n=5 kPa: a) Level I, b) Level II, c) Level III, d) Level IV, e) Level V, f) Level VI: gtxd-13 220

Figure C.29: Comparison between actual and predicted load/displacement curves for the geotextile pulled in the cross-machine direction at σ_n=5 kPa: gtxd-13 221

Figure C.30: Predicted shear stress versus shear displacement curve for the geotextile pulled in the cross-machine direction at σ_n=5 kPa: gtxd-13 221

Figure C.31: Comparisons between actual and predicted displacement curves for the geotextile pulled in the cross-machine direction at σ_n=15 kPa: a) Level I, b) Level II, c) Level III, d) Level IV, e) Level V, f) Level VI: gtxd-14 222

Figure C.32: Comparison between actual and predicted load/displacement curves for the geotextile pulled in the cross-machine direction at σ_n=15 kPa: gtxd-14 223

LIST OF FIGURES -- Continued

Page

Figure C.33: Predicted shear stress versus shear displacement curve for the geotextile pulled in the cross-machine direction at σ_n=15 kPa: gtxd-14 223

Figure C.34: Comparisons between actual and predicted displacement curves for the geotextile pulled in the cross-machine direction at σ_n=35 kPa: a) Level I, b) Level II, c) Level III, d) Level IV, e) Level V, f) Level VI: gtxd-15 224

Figure C.35: Comparison between actual and predicted load/displacement curves for the geotextile pulled in the cross-machine direction at σ_n=35 kPa: gtxd-15 225

Figure C.36: Predicted shear stress versus shear displacement curve for the geotextile pulled in the cross-machine direction at σ_n=35 kPa: gtxd-15 225

LIST OF SYMBOLS

ABR™	Automatic Binary Regulator
AC	Asphalt concrete
b, B	Width of the test specimen
C_1, C_2, C_3	Experimentally determined constants which help describe soil/geosynthetic interaction
d	Thickness of soil/geosynthetic interface layer
D_{85}	Diameter of soil particles at 85% finer
DC	Direct current
Dr	Relative Density
δ	Soil/geosynthetic friction angle
Δx	Length of element
E_m	Elastic modulus for the machine direction
E_x	Elastic modulus for the cross-machine direction
E_z	Elastic modulus for the out-of-plane direction
ϵ	Strain
ϵ_{lat}	Lateral strain
F	Load
F_{peak}	Peak load
F_r	Residual force at L_{eff}

LIST OF SYMBOLS -- Continued

F_{Tmax}	Maximum applied tensile force
gg45	Geogrid, 45 degree direction
ggmd	Geogrid, machine direction
ggxd	Geogrid, cross-machine direction
gtmd	Geotextile, machine direction
gtxd	Geotextile, cross-machine direction
G, G_i	Initial tangent soil/geosynthetic interface shear modulus
G_{mx}	Shear modulus for the machine/cross-machine plane
G_{mz}	Shear modulus for the machine/out-of-plane plane
G_s	Specific gravity of soil solids
G_{xz}	Shear modulus for the cross-machine/out-of-plane plane
H	Length of the test specimen
HDPE	High density polyethylene
HP	Horsepower
i	Node notation
j	Element notation
J	Analytical constant
L	Length of test specimen
L_{eff}	Effective reinforcement length
MD	Machine direction

LIST OF SYMBOLS -- Continued

n	Number of ribs
ν_{mx}, ν_{xm}	Poisson's ratios in the machine/cross-machine plane
ν_{mz}, ν_{zm}	Poisson's ratios in the machine/out-of-plane plane
ν_{xz}, ν_{zx}	Poisson's ratios in the cross-machine/out-of-plane plane
$P_{corrected}$	Corrected load
$P_{measured}$	Measured load
PET	Polyester
ψ_p	Peak soil/geosynthetic interface friction angle
ψ_r	Residual soil/geosynthetic interface friction angle
R_m	Yield stress ratio in the machine direction
R_{mz}	Yield stress ratio in the machine/out-of-plane plane
R_x	Yield stress ratio in the cross-machine direction
R_{xm}	Yield stress ratio in the cross-machine/machine plane
R_{xz}	Yield stress ratio in the cross-machine/out-of-plane plane
R_z	Yield stress ratio in the out-of-plane direction
σ_0	Ultimate reference normal strength
σ_m	Applied stress in the machine direction
$\overline{\sigma}_m$	Ultimate yield strength in the machine direction
σ_{mz}	Applied shear stress in the machine/out-of-plane direction
$\overline{\sigma}_{mz}$	Ultimate shear strength in the machine/out-of-plane plane

LIST OF SYMBOLS -- Continued

σ_n, σ_v	Applied, vertical, normal confinement
σ_x	Applied stress in the cross-machine direction
$\overline{\sigma}_x$,	Ultimate yield strength in the cross-machine direction
σ_{xm}	Applied shear stress in the cross-machine/machine direction
$\overline{\sigma}_{xm}$	Ultimate shear strength in the cross-machine/machine plane
σ_{xz}	Applied shear stress in the cross-machine/out-of-plane direction
$\overline{\sigma}_{xz}$	Ultimate shear strength in the cross-machine/out-of-plane plane
σ_z	Applied stress in the out-of-plane direction
$\overline{\sigma}_z$	Ultimate yield strength in the out-of-plane direction
$\tau_{average}$	Average interface shear stress
τ_{res}	Residual interface shear stress
τ_{ult}	Ultimate interface shear stress
τ_0	Ultimate reference shear stress
u	Displacement
$W_{corrected}$	Corrected width
$W_{initial}$	Initial width
x	Position
X	Distance along length of embedded geosynthetic
XD	Cross-machine direction

ABSTRACT

In recent years geogrids and geotextiles have been evaluated for use as reinforcement in the base course layer of flexible pavement structures. Adding reinforcement to the base layer can help reduce the thickness of the base material or increase the life of the roadway. To understand and quantify potential reinforcement benefit, a program of study that relies on both experimental and modeling studies was devised. The increased use of finite element modeling to simulate material and system behavior has also increased the need for more specialized tests performed on the model components.

The focus of this research was to develop test methods and provide data that can be used for the calibration of constitutive models that describe geosynthetic material parameters and soil/geosynthetic interaction parameters. Calibration of geosynthetic material models required that elastic, inelastic, viscous, direction dependant and repetitive load dependant material properties be defined. To define the soil/geosynthetic interaction characteristics, in-soil (confined) tests were performed.

A large scale test facility was designed and built for performing both in-air and in-soil experiments on geosynthetics. In-air, displacement-rate controlled (monotonic) and load controlled (cyclic) tests on the geosynthetic material allowed orthotropic elastic and isotropic yield material properties to be obtained. Monotonic pull-out tests were performed at three levels of normal confinement to calibrate soil/geosynthetic interaction parameters. Several common methods of interpreting the data from these tests were examined, but, due to complications associated with these methods, a numerical solution of the governing differential equation, which describes the interaction problem, was formulated.

CHAPTER ONE

INTRODUCTION

Background

In recent years, geosynthetics have been used as reinforcement contained in the base course layer of flexible pavements. To quantify potential benefit provided by this reinforcement, understanding the mechanisms of interaction between the geosynthetic and the surrounding base material is essential.

Using geosynthetic materials as reinforcement in the base layer of flexible pavement systems may provide savings either through a reduction of the base course layer design thickness or an extension of the life of the road. Studies ranging from outdoor, field-scale tests to indoor, laboratory-scale tests have been conducted to provide insight into the mechanisms of geosynthetic reinforcement and its level of structural contribution. Reinforcement is derived mainly from the interaction between the base course material and the geosynthetic reinforcement. The goal of ongoing research at Montana State University is to understand and quantify potential reinforcement benefit using laboratory experiments and finite element modeling.

A fully instrumented, laboratory-scale test facility has been constructed to examine geosynthetic reinforcement benefit under simulated, truck traffic loading. This test facility

has allowed a geosynthetic reinforced pavement section to be built on a subgrade material within a controlled environment. In these test sections, cyclic loads were applied to the top of the asphalt concrete (AC) layer through a rigid, 305 mm diameter plate. Two types of geosynthetics were used in this study: a biaxial, polypropylene geogrid and a biaxial, woven, polypropylene geotextile. This phase of the research measured stress and strain response in several layers of the pavement section under these loads. Specifically, stress was measured in the base course and subgrade layers and strain was measured in the AC layer, the base course layer, the geosynthetic layer and the subgrade layer. The modeling portion of this study is being developed to match these observed stress and strain responses. Calibrating the model until it accurately predicts the response seen in these tests will allow a parametric study to be formed to predict responses for variables not included in the actual experiments. Using this parametric study, a design methodology for geosynthetic reinforced pavements can be formulated.

To model the reinforced pavement system properly, material parameters describing each component of the system must be defined. Specifically, the intrinsic geosynthetic material properties and soil/geosynthetic interaction properties must be identified. The focus of this thesis is the development and implementation of a testing scheme that provides the appropriate geosynthetic constitutive material parameters to the finite element model.

Scope of Work

Geosynthetic materials exhibit elastic, inelastic, viscous, direction dependent and repetitive load dependent characteristics. The overall purpose of the research contained in

this thesis is to develop test methods and provide data that can be used to obtain appropriate geosynthetic material properties used in the constitutive model, including base course soil/geosynthetic interaction properties. Specifically, the material parameters needed are:

- Geosynthetic, orthotropic, elastic/plastic material properties.
- Geosynthetic, nonlinear, combined isotropic/kinematic hardening material properties.
- Soil/geosynthetic, elastic/plastic, Coulomb type friction coefficients.

To accomplish this, the following objectives were established:

- Design and commission of an apparatus, based on current design practices, to perform both in-air and in-soil tests under monotonic and cyclic loading.
- Use data from in-air tests to calibrate constitutive geosynthetic material parameters in the finite element model.
- Use data from monotonic in-soil tests to formulate an analytical model to establish a method of interpreting the soil/geosynthetic interaction properties to be used in the finite element model.

Experimentation

To define geosynthetic material and interaction properties properly, performing tests on each of the geosynthetic materials used in the plate-load tests was necessary. To do this, two types of tests were preferred: in-air tests and in-soil tests. Each of these tests was conducted under two types of loading: displacement controlled (monotonic) and load controlled (cyclic). The materials studied were biaxial, implying they have different mechanical properties in each of their principle directions. Accordingly, all tests were performed to define the material's anisotropic characteristics.

In-air Tests

The materials' orthotropic, elastic/plastic material properties were defined using monotonic, in-air tests. In this thesis, an in-air test refers to any laboratory experiment performed on the geosynthetic where no confinement is applied in the out-of-plane direction. Since calibration of the constitutive model requires data corresponding to a state of uniaxial tension, all in-air tests were performed as uniaxial tension element tests. Measurements of applied load, axial strain and lateral strains were collected to calculate moduli values for each of the principle directions. Two types of monotonic tests were performed: fast monotonic and slow monotonic. Fast monotonic tests were performed to provide geosynthetic material parameters without creep. Slow monotonic tests were used to calibrate both the elastic and plastic material properties and verify the finite element model's prediction of creep.

Since the elastic/plastic model, calibrated by the monotonic tests, does not necessarily account for material behavior under cyclic loading, a second model is being developed. This second model is being used to define the materials' nonlinear, combined isotropic/kinematic, hardening material properties. To calibrate this model, geosynthetic samples were cyclically loaded, allowing them to experience ratchetting effects. Ratchetting refers to the accumulation of plastic strains within the material under a particular level of repeated load amplitude. Cyclic tests were carried out on the geosynthetic materials using two types of loading: single cycle step loading (Series I) and multiple cycle step loading (Series II). For the Series I tests, the geosynthetic samples were subjected to one cycle at 14 different levels of load amplitude. For the Series II tests, load cycles were repeated at each of these same

levels of load amplitude until it was determined that plastic strains due to ratchetting were fully developed. The Series I tests were used to further investigate the reliability of the material parameters derived from the Series II tests.

In-Soil Tests

To calibrate the elastic/plastic Coulomb friction law describing the interaction between the base course soil and the geosynthetic, in-soil tests were performed. Like in-air tests, in-soil tests were also conducted under two types of loading: monotonic and cyclic. In-soil tests were performed using a pull-out box. This apparatus allowed an embedded sample of geosynthetic to be pulled from the soil while measurements of applied load and displacement along its embedded length were collected. The soil used in these tests was the same as the gravel base course used in the pavement test facility.

Analyzing soil/geosynthetic interaction along the length of the geosynthetic is complicated by the high elongation of the geosynthetic material during pull-out testing. Since engagement of the sample is progressive, shear stress cannot be directly measured between the soil and the geosynthetic. Several related analysis techniques for determining the soil/geosynthetic interaction parameters have been attempted and used in the past. Each of these methods has been investigated and outlined in Chapter 2. Associated problems with several proposed methodologies influenced the author to develop a method of calculating soil/geosynthetic interaction based on numerical techniques.

The interaction parameters were determined from monotonic tests performed on each geosynthetic material in their principle directions. These tests were performed under three

different levels of normal confinement, since the friction law is normal stress dependant. Data from each of these tests was used within the newly developed numerical analysis to calculate interaction parameters for each of the material's principle strength directions. Data from cyclic, in-soil tests will be used to validate and calibrate finite element predicted, interaction parameters under cyclic loads.

Organization of Thesis

A critical review of existing literature for the design, use and interpretation of data obtained from in-air and in-soil testing facilities is contained in Chapter 2. A detailed description of the design and construction of the apparatus used in this research is included in Chapter 3. Chapter 3 also describes the experimental procedure used for preparing and performing these tests, illustrates corrections made to raw data and gives examples of typical results. A discussion of experimental results and an in depth description of the analytical methods used to determine material and interaction parameters from each of these tests is outlined in Chapter 4. Conclusions drawn from this study and recommendations for further research are made in Chapter 5.

CHAPTER TWO

LITERATURE REVIEW

Introduction

The literature review in this chapter consists of two main sections; in-air testing and in-soil testing of geosynthetics. Each section includes a discussion of previous apparatus design, test procedures, and analysis of results. Problems associated with existing test methods and analyses are also discussed.

In-Air Testing

Due to the various factors affecting results obtained from in-air tests, careful consideration must be given to the design and construction of an in-air apparatus. In this review, four areas are considered: 1) the overall geometry of the test specimen, 2) the method of applying the load, 3) the method of gripping the sample and 4) the temperature during testing.

Many geosynthetics experience necking under uniaxial loading. To reduce this effect, sample widths are typically increased so that the experimental setup mimics a plane-strain condition. This condition has been argued to be more closely related to field applications (ASTM, 1995) where geosynthetics in tension are generally very wide. However, calibration

of a constitutive model requires data corresponding to a state of uniaxial tension. Samples pulled under plane-strain conditions may yield different results than samples pulled uniaxially. Samples with a small aspect ratio resemble uniaxial loading since material in the direction of the sample's width is much smaller than the length, therefore reducing its effect on load/strain properties. Choosing a sample size that ensures a state of uniaxial tension over the central region of the sample allows axial and lateral strains to develop freely without influence from the ends. Measured lateral strains allow the load to be corrected for changes in width due to Poisson effects.

Changes in sample geometry have been shown to affect the measured properties of geosynthetics. Myles (1987) showed that strength per unit width decreased in a geotextile when the aspect ratio (B/H) was lowered, where B and H are the width and height (or length) of the test specimen, respectively. Rowe and Ho (1986) showed that initial tangent modulus values for a woven geotextile stayed relatively constant under different aspect ratios. Figure 2.1 illustrates that tangent modulus values from 5-10% axial strain decreased as the aspect ratio became larger.

Both strain-rate controlled and displacement-rate controlled test apparatuses are used to determine the load-strain behavior of geosynthetics. Geosynthetic materials are known to be load-rate sensitive materials. Rowe and Ho (1986) showed that the maximum tensile strength of geotextile materials is quite sensitive to strain rates, where increased strain rate increases the maximum tensile strength, as shown in Figure 2.2. Bathurst and Cai (1994) found that increased loading rate of an HDPE geogrid increased secant and tangent moduli values and its ultimate strength (Figure 2.3). When load magnitudes are applied in a cyclic